IOP Publishing Journal of Physics: Condensed Matter
J. Phys.: Condens. Matter **29** (2017) 504002 (8pp) https://doi.org/10.1088/1361-648X/aa99c6

Membrane vesiculation induced by proteins of the dengue virus envelope studied by molecular dynamics simulations

Ricardo de Oliveira dos Santos Soares[1,2], Leandro Oliveira Bortot[2], David van der Spoel[3] and Antonio Caliri[2]

[1] Faculdade de Medicina de Marília, Marília, Brazil
[2] Faculdade de Ciências Farmacêuticas de Ribeirão Preto, Departamento de Física e Química, Grupo de Física Biológica, Universidade de São Paulo, Ribeirão Preto, Brazil
[3] Department of Cell and Molecular Biology, Uppsala Centre for Computational Chemistry, Science for Life Laboratory, Uppsala University, Box 596, SE-75124 Uppsala, Sweden

E-mail: ancaliri@fcfrp.usp.br

Received 30 August 2017, revised 10 November 2017
Accepted for publication 10 November 2017
Published 24 November 2017

Abstract

Biological membranes are continuously remodeled in the cell by specific membrane-shaping machineries to form, for example, tubes and vesicles. We examine fundamental mechanisms involved in the vesiculation processes induced by a cluster of envelope (E) and membrane (M) proteins of the dengue virus (DENV) using molecular dynamics simulations and a coarse-grained model. We show that an arrangement of three E-M heterotetramers (EM_3) works as a bending unit and an ordered cluster of five such units generates a closed vesicle, reminiscent of the virus budding process. *In silico* mutagenesis of two charged residues of the anchor helices of the envelope proteins of DENV shows that Arg-471 and Arg-60 are fundamental to produce bending stress on the membrane. The fine-tuning between the size of the EM_3 unit and its specific bending action suggests this protein unit is an important factor in determining the viral particle size.

Keywords: dengue, virus, simulation, GROMACS, envelope

S Supplementary material for this article is available online

(Some figures may appear in colour only in the online journal)

Introduction

The mechanisms of membrane remodeling in the cell constitute a fundamental problem in molecular biology [1] with important applications in different areas of science and technology, such as nanomedicine, synthetic molecule carriers, new vaccine development, and material sciences [2–6]. Biological membranes consist of phospholipid bilayers with embedded integral and peripheral proteins that can rotate and translate laterally. Membranes may attain curvature as a consequence of asymmetry imposed by its own constituents, such as cholesterol, or by the presence of external molecules, such as proteins that can insert hydrophobic domains into one side of the bilayer with membrane-piercing α-helices [7]. This type of helix can hook the opposite side of the membrane and produce a local constriction on membrane thickness or they may act as scaffolds for membrane curvature [1, 8, 9]. Moreover, domains of different lipids or clusters of proteins, as well as the boundaries of an open membrane, may produce lines of tension that introduce extra forces on the membrane [10, 11].

Replication of enveloped viruses comprises several steps controlled by specific proteins. These include local membrane bending [1] followed by virus budding and final membrane scission, in which the virion is detached from the cellular membrane [12]. Specifically, the dengue virus (DENV)

[13, 14] is coated by replicas of two proteins, namely envelope (E) and membrane (M) proteins, forming 90 E-M heterotetramers (2 E + 2 M) that cover a spherical phospholipid membrane. The E protein presents a soluble ectodomain (sE) and a transmembrane domain (TMD) that acts as an anchor. The M protein resides under the E protein shell, practically immersed in the virus membrane (figures 1(A) and (B)). The transmembrane domain of the E-M heterotetramer is subdivided into stem and anchor helices (figure 1(A)); the stem helices have a polar/nonpolar surface pattern and are all accommodated at one side of the bilayer surface, while the anchors, mostly hydrophobic, present polar residues only at their distal loops [14–16]. Theses loops connect two helices of the E protein (ET1; ET2) and two helices of the M protein (MT1; MT2).

A set of high-resolution structures of the DENV-2 envelope proteins [14, 15, 17] allows us to use molecular dynamics (MD) simulations to investigate the effects of protein-protein and protein-membrane interactions in the generation of membrane-bending forces. Here, we examine deformations induced on a host-like phospholipid bilayer [18] (see Methods section) in a progressive way, through three distinct oligomerization states of E-M proteins, namely: one (EM_1), three (EM_3), and fifteen (EM_{15}) heterotetramers (figures 1(C)–(E)). Essentially, this work concerns the description and analysis of the membrane bending and vesiculation mechanisms induced by the envelope proteins of the DENV. The EM_{15} system emulates a fragment of the DENV envelope: it is composed of an open membrane patch of $59 \times 59\,nm^2$ encrusted by 1/6 of the outer structural proteins of DENV immersed in solvent particles, amounting to the equivalent of three million atoms.

Our results show that the E-M heterotetramer architecture has a key topological and physicochemical characteristic that ultimately breaks the planar symmetry of the bilayer and generates forces capable of modifying the overall bilayer shape. We present *in silico* mutagenesis experiments that corroborate the notion that the membrane-bending forces are a consequence of the phospholipid rearrangement triggered by the relatively short length of the TMD of the E-M proteins. As more E-M heterotetramers are assembled in a symmetric setup, the resulting curvature in the planar phospholipid bilayer leads to a self-assembled vesicle, impelled by the accumulated mechanical stress imposed by the proteins and also by a line of tension along the membrane boundary.

Methods

Molecular dynamics (MD) simulation and analysis

All MD simulations in this work were performed using the GROMACS 4 package [19]; the CHARMM36c [20] force field with cholesterol parameters [21] and TIP3P water [22] was used to supply the energy function for all-atom (AA) MD simulations. The MARTINI [23] model was used for the coarse-grained (CG) modeling. All bilayers in this work emulate the phospholipid composition of the DENV membrane [24]. The method described in Hsin *et al* [25] was employed to evaluate the bilayer curvature. Analyses, visualization, and preparation of figures were performed through the following tools: GROMACS, VMD [26], and open-source PyMol [27]. The complete methodology is described in the separated topics below.

System preparation: general aspects

All atom simulations for EM_1 and EM_3 systems and CG 'simulations' for EM_3 and the large EM_{15} system were performed. We write 'simulations' since the CG energy function is a mixture between enthalpy and entropy. This mix-up leads to the problem that the 'forces' in a CG model include the time derivative of the entropy (the same goes for implicit solvent models). Hence CG can not be used to generate simulation trajectories, the resulting ensemble is not a Boltzmann ensemble and the concept of time is ill-defined. CG 'simulations' should therefore be considered as an algorithm to search the free energy landscape. For readability we leave out the '' in the remainder of the text.

The phospholipid composition of the bilayer model follows the actual ratios in DENV, derived from the mosquito lipidome [24]: POPC (1-palmitoyl-2-oleoyl-*sn*-glicero-3-phosphatidylcholine), 60%; POPE (1-palmitoyl-2-oleoyl-*sn*-glicero-3-phosphatidylethanolamine), 20%; and POPS (1-palmitoyl-2-oleoyl-*sn*-glicero-3-phosphatidylserine), 10%. The remaining 10% corresponds to the cholesterol fraction, as found on mammalian RER membranes [28]. The system's net charge was neutralized by the addition of Na^+ and Cl^- counter ions at the ionic strength of 150 mM.

The geometry of molecules and their interactions were optimized after protein embedding by performing energy minimization with the steepest descent method. Position restraints were applied to a set of system-dependent atoms during equilibration runs. A Maxwell–Boltzmann distribution was used to generate the initial velocities of the atoms at a temperature of 310 K and thermal stabilization was achieved using the Berendsen thermostat [29]. The cutoffs of nonbonded interactions were set to 1.0 nm for AA simulations or 1.2 nm for CG simulations. Long-range electrostatic interactions were dealt with using the particle-mesh Ewald method, with sixth order interpolation. Bonds containing hydrogen atoms were constrained by the LINCS [30] algorithm, except when minimizing the potential energy of CG beads in the presence of polarizable water [31].

We used the replacement method for protein insertion [32] in all cases; the AA bilayers were equilibrated prior the insertion, while the CG bilayers were equilibrated after protein insertion using position restraints on the protein. For the AA equilibration steps we used the Berendsen algorithm [29] to control both temperature (310 K) and pressure (1 bar); for production we used the Berendsen barostat to control surface tension (NPγT ensemble, $\gamma = 0$) and V-rescale [33] for temperature coupling. Periodic boundary conditions in a semi-isotropic regime were applied in EM_1 and EM_3 systems; the membrane covered the entire cross-section of the simulation box. Open membrane patches were used for the larger EM_{15} system, and this was simulated with isotropic periodic boundary conditions. The time step for leap-frog algorithm integration was set to 1 femtosecond (fs) and 20 fs for AA and

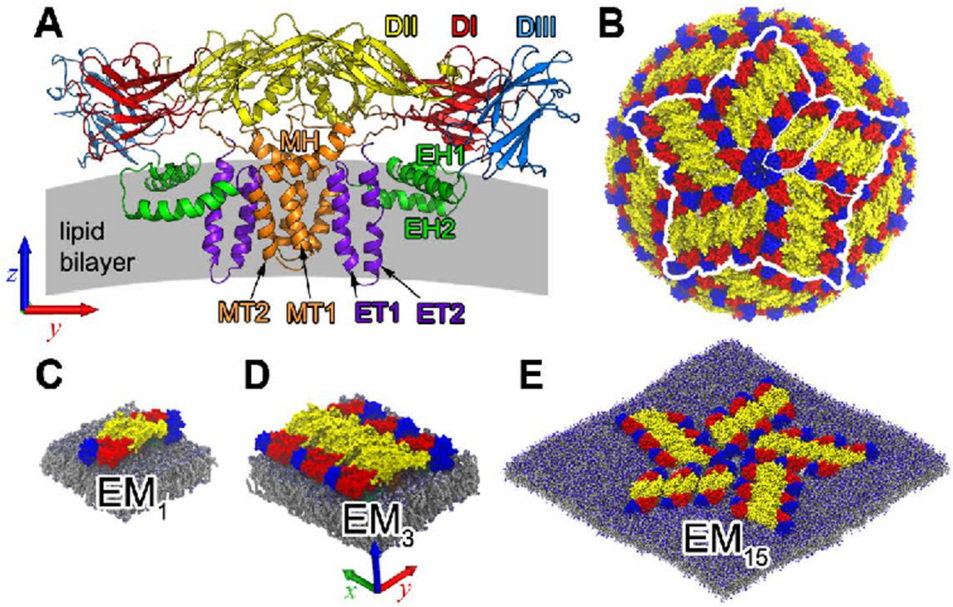

Figure 1. Envelope (E) and membrane (M) proteins of the dengue virus (DENV). (A) Structures of the EM heterotetramer (two E and two M) of DENV: domain I (DI, red), domain II (DII, yellow), and domain III (DIII, blue) are the three domains collectively called ectodomain of E. The TMD is composed of (i) stem: six helices (two sets each of EH1, EH2, and MH) partially embedded into the bilayer, and (ii) anchor: eight membrane-piercing helices (two sets each of ET1, ET2, MT1, and MT2). (B) Structural surface of DENV as crystallographically determined; note the fivefold axis at the center of the figure (blue circle-like spot). White lines highlight the three systems considered here, composed of one (EM_1), three (EM_3), and fifteen (EM_{15}) EM heterotetramers. (C) EM_1 system: one EM heterotetramer anchored in a flat continuous membrane connected with its images through the periodic boundary conditions. (D) The EM_3 system corresponds to three EM_1 shaped as an irregular rhombus also planted parallel into the flat 'continuous' membrane. (E) In turn, the EM_{15} system (shown in smaller scale here) consists of five groups of EM_3, facing each other in a rotationally symmetric fashion, embedded into a flat open membrane patch of size $59 \times 59\,nm^2$. It reproduces a planar version of the cluster of fifteen EM heterotetramers around the fivefold axis of the icosahedral symmetry of the DENV.

CG simulations, respectively. For consistency with other literature all reported MD-times for CG simulations were multiplied by a factor of four to represent an estimate of real time [23], however with the caveat noted above that there is no time in CG simulations. Analyses of bilayer curvature were performed with a method described by Jen Hsin [25] who kindly provided a script for this purpose.

EM_1 system

The EM_1 system is a heterotetramer composed of a single set of two E and two M proteins embedded in a flat bilayer patch measuring $14.8 \times 14.8\,nm^2$ and with a thickness of about 4 nm. Periodic boundary conditions were employed to emulate a continuous membrane (figure 1(C)), by replication of the original square patch in the *x*- and *y*-direction.

The AA model of the DENV E-M heterotetramer (serotype 2) was obtained from the RCSB Protein Data Bank [34] under the accesion code 3J27 [14]. This model is derived from an electron microscopy structure with resolution of 3.5 Å and contains all amino acids of the native E and M proteins. We extracted the atoms that correspond to one E-M heterotetramer and added all missing hydrogen atoms. Then, we performed a steepest-descent energy minimization, removing eventual steric impairments on the structure.

The lipid bilayer was assembled with aid of the membrane builder module from CHARMM-GUI [35]. The resulting bilayer initially contained 800 phospholipid and cholesterol molecules equally divided between its upper and lower layers. First, we removed all overlapping phospholipid acyl chains with a series of steepest-descent energy minimizations in conjunction with the *inflategro* script [32]. Then, we solvated the bilayer with the TIP3P CHARMM water model [36] with a water/lipid weight ratio (%wtH_2O) above the phase transition threshold of the liquid crystal state (Lα), with an experimental value [32] of 32.5. In order to equilibrate the solvent layer at the interface of the membrane, we performed a 5 ns equilibration in the NVT ensemble using position restraints on the phosphor atoms of the lipids to allow diffusion only in the *xy* plane.

Another 10 ns thermalization under the NPT ensemble without restraints was performed, adjusting the box to yield a system pressure of 1 bar using the Berendsen barostat [29] with $\tau_P = 1$ ps. In the final step, we adjusted the surface tension to zero under the NPγT ensemble with the Berendsen algorithm for 60 ns. The temperature of the system was maintained within the physiological threshold and above the transition temperature of the bilayers components to achieve the Lα phase of a typical biological membrane. The expected reference properties were confirmed by establishing the approximate area per lipid of $0.55\,nm^2$, the average bilayer thickness of 4.3 nm and the characteristic order of the lipids acyl chains, as described by the lipid deuterium order parameter and electronic density of the system. After protein embedding, a 10 ns equilibrium run was performed with restraints on the heavy atoms of the protein, allowing the bilayer to fully embed the

TMD. Then, we proceeded with the production run of 100 ns under the NPγT ensemble.

EM_3 systems

To obtain the EM_3 system, the coordinates of three neighboring heterotetramers in the biological assembly were extracted from the same cryo-EM structure used for EM_1. The three heterotetramers were put in the same plane of reference, obtaining a planar configuration. To accommodate these three heterotetramers, a larger bilayer fitting a box $20.8 \times 14.6 \times 13.8\,nm^3$ was taken from the previously equilibrated membrane and an additional layer of water was added, yielding $\%wt_{H_2O} \sim 91$. Then a 60 ns NPγT equilibration was carried out with the same parameters as the smaller bilayer to thermalize the system. Finally, we proceeded with the production run of 100 ns under the NPγT ensemble.

To convert the AA EM_3 configuration to a CG model, we employed the *martinyze* script [23]. The lipid bilayer and solvated box, with polarizable water [31], was built with MARTINI's *insane* script [23]. The first step in the process of embedding the TMD into the bilayer consisted of the alignment of both geometrical centers of the proteins and bilayer in the *XY*-plane. Next, the TMD were adjusted along the *Z*-axis as close as possible to the bilayer depth described in the cryo-EM structure. At this stage, all overlapping non-protein molecules within a distance smaller than 1.2 Å of the heterotetramer were removed. After the addition of Na^+ and Cl^- to achieve the desired ionic strength and electroneutrality, we proceeded to a steepest-descent energy minimization, and the resulting system was used as the starting conformation for a 10 ns NVT step in which protein atoms were restrained in their positions and the phosphor atoms of each phospholipid were allowed to laterally diffuse through the membrane. Then, all restrictions were released and the 100 ns production run started.

Two CG EM_3 systems for *in silico* mutation simulations were prepared: one consisted of a single mutation from Arg-471 to Ala in the E protein and the other with an extra mutation of Arg-60 to Ala in the M protein. These substitutions were performed directly on the heterotetramers on the starting structure of the AA EM_3, using the mutagenesis tool of Pymol [27]. Then, the resulting AA file was converted to a CG system model with the *martinize* script [23]. From there, all steps were identical to the CG EM_3 system assembly, equilibration, and production of 100 ns.

EM_{15} system

The EM_{15} system was built on an open membrane patch of area $59 \times 59\,nm^2$, consisting of 8008 lipids and 856 cholesterol molecules, in a box of size $62.9 \times 62.9\,nm^2$. The number of lipids molecules and cholesterol molecules in the upper layer was about 22% less than in the lower layer, due to the surface area S_p occupied by the protein cluster. Five EM_3 structures constituted the building blocks of the EM_{15} system, forming a cluster of 15 E-M heterotetramers. Note

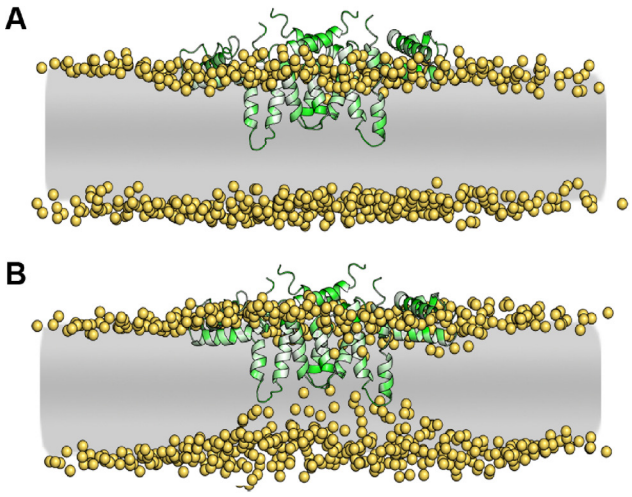

Figure 2. Evolution of the interplay between the EM heterotetramer and membrane. (A) The initial conformation corresponding to the embedding of the TMD of the EM heterotetramer, placing the amphipathic stem helices (EH1, EH2 and MH) inside the hydrophobic lipid matrix of the membrane, a thermodynamically unfavorable condition—the golden spheres represent the polar heads of phospholipid molecules. (B) pronounced indentation on the lower phospholipid layer caused by the TMD.

that six such raft-like domains are needed to cover the entire DENV (figures 1(B) and (E)). The lines coming out from the DENV five fold symmetry axis and passing through domain II of the ectodomain of protein E of each EM_3 (figures 1(B) and (E), colored yellow), define the five arms of the EM_{15} system. Each EM_3 block bends the membrane along each arm of the EM_{15} cluster.

The E-M heterotetramers are initially arranged as a planar projection of the coordinates of the fivefold pore of the cryo-EM structure, figure 1(E). They correspond to the five CG EM_3 initial systems, as described above, with each EM_3 structure successively rotated by 72° around its *Z*-axis, with respect to the preceding structure. After embedding the proteins into the bilayer and removing all overlapping molecules of the membrane, we proceeded with the same equilibration steps described in the CG EM_3 bilayer, and another 10 ns of NPT run with protein coordinates fully restrained, allowing the stabilization of pressure to the NVT production run, for 150 ns (CG time).

Results and discussion

Origin of bending forces

The E and M proteins of *Flavivirus* have two short bisected helices. In the case of DENV, the anchor helices ET1 and ET2 are 16 and 17 residues long, respectively, whereas they are only 12 and 14 residues long for MT1 and MT2, respectively. Initially, the TMD of the E-M proteins was aligned closely to the upper layer of a continuous membrane (figure 2(A); see also the Methods section); this configuration is thermodynamically unfavorable because the anchor helices, which are relatively short, have their polar loops in a hydrophobic environment (the middle portion of the membrane). Therefore,

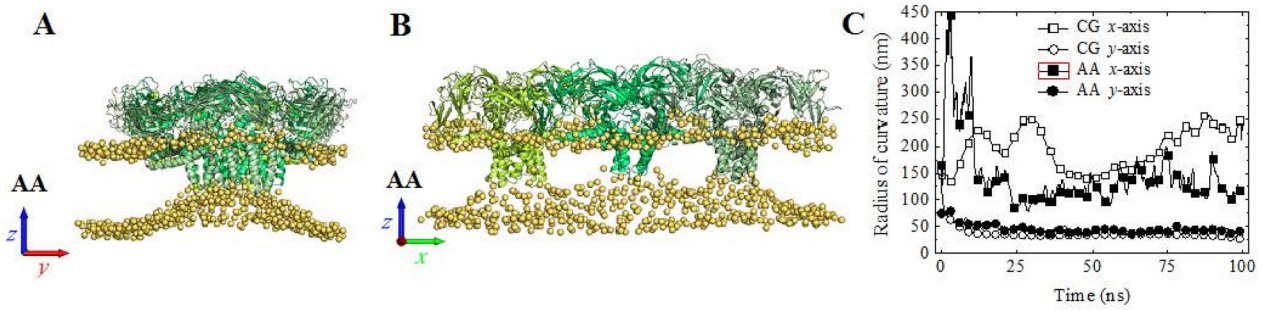

Figure 3. Membrane curvature produced by the EM_3 system (a trimer of EM heterotetramers). (A) Full all-atom simulation of three aligned EM heterotetramers as in the DENV native conformation (each colored in different shades of green for distinction). After 100 ns the system reaches stable conformation, with the membrane bilayer keeping an asymmetric curvature exclusively along a specific direction (y-axis). (B) The same, but with view orientation along the x-axis of the simulation box: the overall curvature is practically zero. (C) Evolution of the radius of curvature, represented by the two layer local average about the protein cluster center: all-atom (AA) simulation (full symbols) and coarse-grained (CG) model (open symbols) of the EM_3 system. Both methods reproduce the same anisotropic curvature in the y-axis direction, corresponding to the DENV radius (25 nm). The gain in performance using the CG method is about 18 times faster.

a prompt rearrangement of the lipids molecules and cholesterol molecules takes place, producing a local constriction on the membrane: the bottom layer is attracted by the polar tip of the anchor helices, pulling down the whole TMD, which gets embedded deeper into the membrane, pressuring the upper monolayer. Promptly, the E-M heterotetramer becomes attached to the membrane through the amphipathic EH1, EH2, and MH helices. Concomitantly, the lipid rearrangement leads to a number of polar phosphate groups from the bottom layer to move toward the polar helices' loops. After about 50 ns, the system is stabilized in a conformation that shows an upper planar layer and a bottom layer containing an indentation right below the TMD (figure 2(B)), which leads to a locally reduced thickness of the bilayer. This is in good agreement to the experimental observation made using cryo-electron microscopy that the membrane thickness is reduced by the transmembrane helices of E and M [14].

A cluster of three EM heterotetramers induces a defined bilayer curvature

Simulations of the AA EM_3 system, which consists of a continuous bilayer over which the EM heterotetramers are positioned as they are found in the mature form of DENV [37] (figure 1(D), details in the Methods section), reveal an intensified curvature of the membrane bilayer, exclusively pronounced in the direction perpendicular to the longest axis of an EM heterotetramer (figures 1(A) and 3(A), labeled here as the y-axis direction). In turn, along the x-direction, the overall curvature is practically zero (figure 3(B)). The local radius of curvature R_C observed along the y-axis, just at the middle of the protein cluster, converges asymptotically to the actual radius of the mature DENV particle [14] $R_{virus} \approx 25$ nm (figure 3(C), full symbols). R_C corresponds to the average between the internal and external bilayer radii of curvatures. This result suggests that, by imposing a defined curvature upon the membrane, the transmembrane helices of the EM_3 cluster may be a key factor in determining the virus size as well as the number of its envelope components.

The fundamental role of two arginine residues

The membrane curvature for the wild-type EM_3 was reproduced using a CG approach (figure 3(C), open symbols), resulting in a 18-fold lower computational cost. This was exploited to verify the effect of mutating two positively charged residues on the ability of the EM_3 system to bend the membrane. Arg-471 and Arg-60 are located at the loops of the anchor proteins (figure 1(A)) and were changed as (i) a single mutation of Arg-471 to Ala; and (ii) double mutation of both Arg-471 and Arg-60 to Ala.

The mutants resulted in a drastically reduced attraction of the lower layer by the anchor loops and the curvature imposed by the wild-type EM_3 system is not observed in the mutants (figure 4). This suggests that these two arginines are fundamental for the function of the envelope proteins. Without them, the EM_3 heterotetramer loses its capacity to impose a curvature upon the membrane, which could impair virus assembly and budding.

Total vesiculation of an open membrane patch induced by 15 EM heterotetramers

The EM_{15} system consists of five EM_3 structures, forming a cluster of fifteen EM heterotetramers, accounting for one sixth of the domains covering DENV. The EM_3 elements are arranged as a planar version of the cluster of proteins around the fivefold axis of DENV (compare figures 1(B) and (E)). The orientation of the curved surface of each EM_3 element (y-direction, figures 1(A) and 3(A)) is perpendicular to its correspondent arm. The EM_{15} system is built on an open membrane patch (more details in the Methods section).

The first change in the morphology of the open membrane patch is that the edges, initially shaped like a square wafer (figure 5(A)), begin to round of in order to reduce the contact area between the hydrophobic tail of the lipids and water (figure 5(B)). Concomitantly, the EM_{15} system starts to impose a specific curvature on the membrane, breaking its initial symmetry (upper and lower different leaflet curvatures), which is minimized by transferring lipid molecules from the lower into

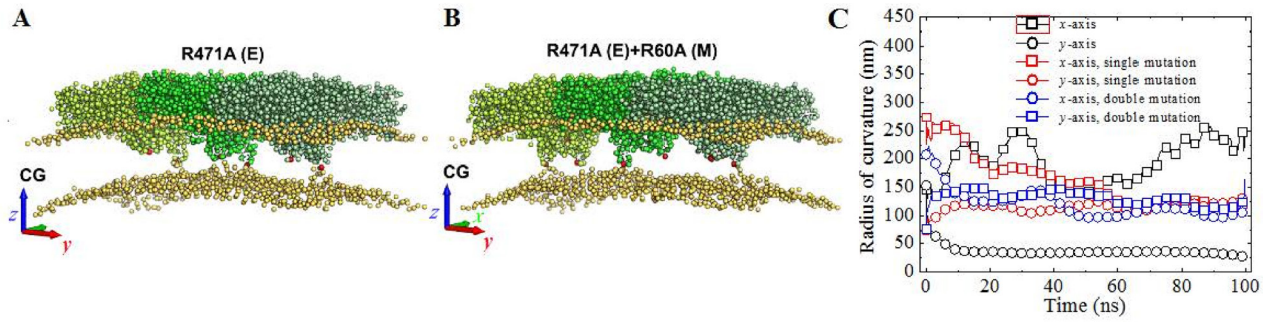

Figure 4. *In silico* mutagenesis of the EM_3 system: the arginine-to-alanine replacement eliminates the bending capability of the EM heterotetramers. (A) When only the Arg-471 in E protein is replaced (colored in red), the membrane curvature becomes instable in both *x*- and *y*-axes (square and circle colored red in (C)), oscillating around a much larger radius of curvature. (B) On the other hand, when both Arg-471 in E and Arg-60 in M protein are substituted, the membrane curvature becomes totally undefined (square and circle colored blue in (C)) changing randomly in both *x* and *y* directions. (C) Evolution of the radius of curvature (CG simulation). Blue symbols, double mutations: R471 + R60A; read symbols, single mutations: R471A; and black symbols: no mutation. Note that only the wild case produces a defined anisotropic curvature in the *y*-direction as in the AA simulation (figures 3(A) and (C)).

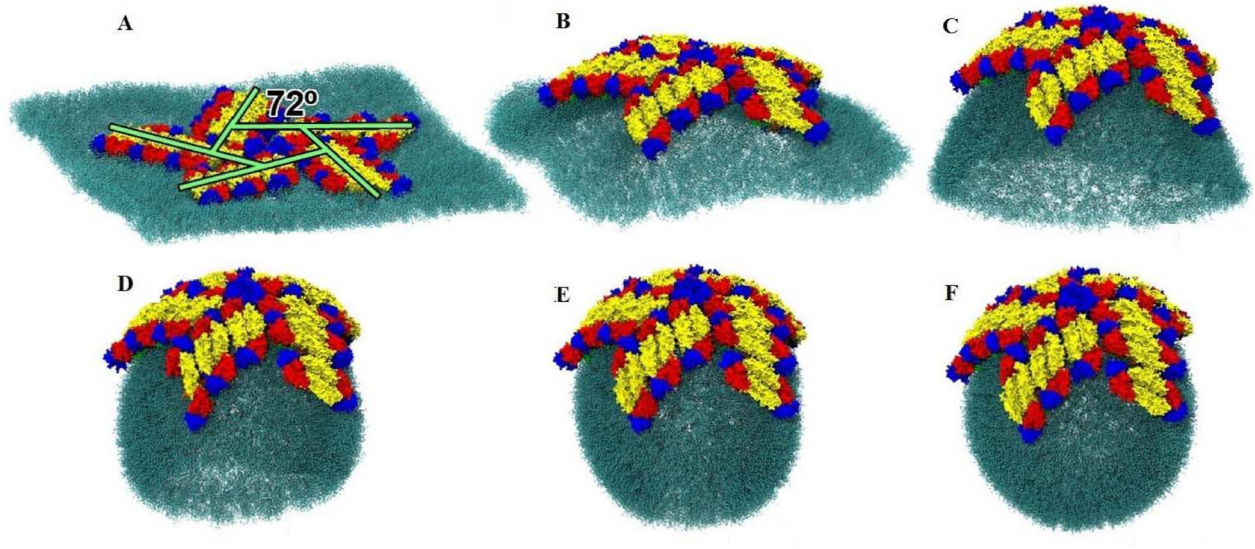

Figure 5. The vesiculation process. (A) The EM_{15} setup: fifteen EM heterotetramers on a flat membrane patch of $59 \times 59\,nm^2$. (B) After 80 ns the membrane already shows a defied curvature, induced by the protein-membrane interplay and by the line of tension around the membrane. (C) The curvature grows systematically and about 240 ns later, a parabolic-like cap is formed. At this stage, the protein-membrane interaction reaches a steady conformation and thereafter, the vesiculation evolutes exclusively under action of the line tension. (D) and (E) As time goes on, the membrane curvature continues to decline. Note that the curvature determined by the protein-membrane interaction (on the top of the sphere) is smaller than the curvature determined by the rest of the membrane. (F) The vesicle reaches a final stable size (external radius of 17.3 nm) at about 440 ns. A comparison between parts (C) and (F) can show how the radius of curvature decreased.

the upper layer. Tension is also accumulated along the membrane rounded edge, which forces to reduce its perimeter; see Movie-1 and 2, in supplementary material (stacks.iop.org/JPhysCM/29/504002/mmedia). Therefore, the bilayer evolves continually as a spherical cap (figures 5(D) and (E)) until the point in which its opening becomes sufficiently small to allow thermal fluctuations to fuse the membrane (figure 5(F)). This process generates a vesicle of external, internal and average radii of $R_{out} = 17.3$ nm, $R_{in} = 13.3$ nm and $R = 15.3$ nm.

The composition and the surface density of molecules on the membrane layers change notably during the vesiculation process due to migration of lipids from the inner layer, which lost 18% of its lipids, to the outer layer, which received additional 24% of its initial number of lipids (figure 6). The overall impact of such migration is a decrease of 16% in the total area occupied by all lipids and, as one would expect, a corresponding increase in 19% in lipid density in the whole vesicle. This behavior is, however, asymmetric between the layers: while the inner layer area decreases 36% and its density—defined as the number of lipid head groups per unit area of the membrane—increases 28%, the outer layer shows a different behavior due to the large number of lipids that it accepted during vesiculation; its area expanded by 10% and its lipid density also increased by 12% (figure 6). Cholesterol specifically localizes in the inner layer, where its proportion is 11% higher than in the open patch (figure 6).

Even though this is a large overall change on the membrane surface area, no elastic energy is stored due to membrane

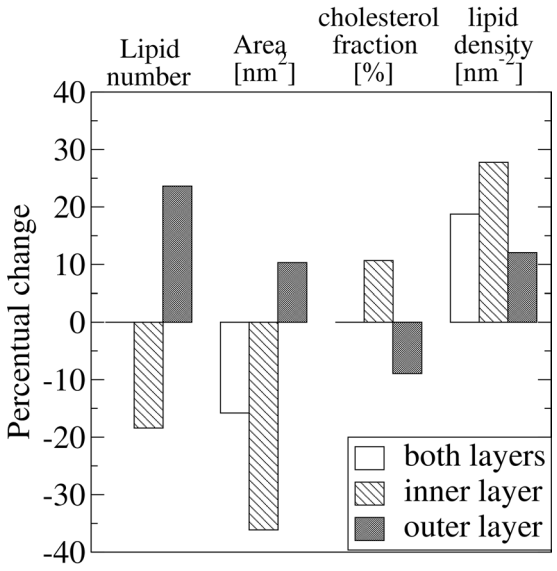

Figure 6. Changes in the membrane layers composition (%) during the observed vesiculation process, in which the number of lipids and cholesterol molecules are preserved in the membrane. The lipid number and area of the outer (dark columns) and inner (hatched columns) layers change asymmetrically: the outer becomes bigger than inner layer, but the lipid density increases in both, markedly in the inner (28.6%). The cholesterol fraction (#chol/#lipids) increases in the inner and diminishes in the outer layer, but the density of lipids incresses in both layers.

deformation because the bilayer is no longer symmetric—a spontaneous curvature was generated during the vesiculation process.

Conclusion

In this work we used molecular dynamics simulations and a coarse-grained model to investigate some aspects of how protein-lipid interactions can shape membranes. The origin of membrane-bending forces was identified by analyzing the behavior of EM, an heterotetramer containing two dimers of the E and M proteins from DENV. This system was considered in three progressively higher oligomerization states assembled in a host-like model membrane.

The structural organization of the EM_3 system—composed by three heterotetramers EM—acts as a anisotropic bending unit for the dengue virus envelope, mainly due to the fact that it can locally reduce the thickness of the membrane with its short transmembrane helices, imposing a specific radius of curvature to the membrane that, locally, at the center of the EM_3 cluster, is similar to that of the DENV, R_{virus} 25 nm. This suggests that the EM_3 unit may be the main determinant of the viral particle size. *In silico* mutagenesis experiments point out that residues Arg-471 and Arg-60 are the responsible for locally reducing the thickness of the bilayer. It will be interesting to see to which extent these specific mutations can impair virus assembly and budding *in vitro* or *in vivo*.

Our simulations show that just a fraction of the envelope proteins of DENV, the EM_{15} system, which corresponds to one sixth of the viral envelope, is competent to induce complete vesiculation of an open membrane patch. The topological pentagonal arrangement of five EM_3 units, acting in concert, imposes a specific curvature R^{-1} to the membrane, breaking its initial symmetry and creating stress in the membrane. Then, the process evolutes spontaneously: the resulting elastic energy is minimized by the systematic migration of lipids from the lower into the upper layer. The lipid transfer is processed exclusively through the edge creating tension along the edge. Such tension is released by continuous reduction of the spherical cap perimeter in formation, and concurrently more lipids are moved to the external layer.

The local curvature R^{-1}_{virus} that the EM_{15} structure seems to impose to the membrane approaches to that of DENV spherical surface. However, R^{-1}_{virus} is larger than the curvature of the vesicle at the simulation end—as one can see by direct inspection of figures 5(D)–(F), since that the vesicle size is limited by the amount of lipids in the initial path.

In short, the vesiculation process studied in this work revels the role of the envelop proteins of DENV in the mechanism of membrane shaping, and the extensive effect the forces of such proteins on the lipid membrane creating enough stress that eventualy transform a flat membrane in an almost perfect sphere tension free.

Acknowledgments

We thank financial support from the Brazilian research funding agencies CAPES, CNPq and FAPESP and the Swedish Research Council for a grant to DS (2013-5947). The hardware, a BlueGene/P cluster, was accessed through a scientific agreement between the University of São Paulo, Brazil, and Rice University, USA.

ORCID iDs

David van der Spoel https://orcid.org/0000-0002-7659-8526

References

[1] Zimmerberg J and Kozlov M M 2006 How proteins produce cellular membrane curvature *Nat. Rev. Mol. Cell Biol.* **7** 9–19
[2] Meyer R A and Green J J 2016 Sharing the future of nanomedicine: anisotropy in polymeric nanoparticle design *WIREs Nanomed. Nanobiotechnol.* **8** 191–207
[3] Yuanzheng W, Hetong Y and Hyung-Jae S 2014 Encapsulation and crystallization of Prussian blue nanoparticles by cowpea chlorotic mottle virus capsids *Biotechnol. Lett.* **36** 515–21
[4] Sánchez-Rodríguez S P *et al* 2016 Enhanced assembly and colloidal stabilization of primate erythroparvovirus 1 virus-like particles for improved surface engineering *Acta Biomater.* **35** 206–14
[5] Soltani F, Parhiz H, Mokhtarzadeh A and Ramezani M 2015 Synthetic and biological vesicular nano-carriers designed for gene delivery *Curr. Pharm. Des.* **21** 6214–35
[6] Mansour A A, Sereda Y V, Yang J and Ortoleva P J 2015 Prospective on multiscale simulation of virus-like particles:

application to computer-aided vaccine design *Vaccine* **33** 5890–6
[7] Derganc J, Antonny B and Čopič A 2013 Membrane bending: the power of protein imbalance *Trends Biochem. Sci.* **38** 576–84
[8] McMahon H T and Gallop J L 2005 Membrane curvature and mechanisms of dynamic cell membrane remodeling *Nature* **438** 590–6
[9] Kirchhausen T 2012 Bending membranes *Nat. Cell Biol.* **14** 906–8
[10] Liu J, Kaksonen M, Drubin D G and Oster G 2006 Endocytic vesicle scission by lipid phase boundary forces *Proc. Natl Acad. Sci. USA* **103** 10277–82
[11] Lipowsky R 1992 Budding of membranes induced by intramembrane domains *J. Phys.* II **2** 1825–40
[12] Welsch S, Miller S, Romero-Brey I, Merz A, Bleck C K, Walther P, Fuller S D, Antony C, Krijnse-Locker J and Bartenschlager R 2009 Composition and three-dimensional architecture of the dengue virus replication and assembly sites *Cell Host Microbe* **5** 365–75
[13] Reddy T and Sansom M S P 2016 The role of the membrane in the structure and biophysical robustness of the dengue virion envelop *Structure* **24** 375–382
[14] Zhang X K, Ge P, Yu X K, Brannan J M, Bi G Q, Zhang Q F, Schein S and Zhou Z H 2013 Cryo-EM structure of the mature dengue virus at 3.5 Å resolution *Nat. Struct. Mol. Biol.* **20** 105–10
[15] Kuhn R J *et al* 2002 Structure of dengue virus: implications for Flavivirus organization, maturation, and fusion *Cell* **108** 717–25
[16] Soares R O S and Caliri A 2013 Stereochemical features of the envelope protein domain III of dengue virus reveals putative antigenic site in the five-fold symmetry axis *Biochim. Biophys. Acta* **1834** 221–30
[17] Kostyuchenko V A, Zhang Q, Tan J L, Ng T-S and Lok S M 2013 Immature and mature dengue serotype 1 virus structures provide insight into the maturation process *J. Virol.* **83** 7700–7
[18] Kozlov M M 2010 Joint effort bends membrane *Nature* **463** 439–40
[19] Pronk S *et al* 2013 GROMACS 4.5: a high-throughput and highly parallel open source molecular simulation toolkit *Bioinformatics* **29** 845–54
[20] Klauda J B, Venable R M, Freites J A, O'Connor J W, Tobias D J, Mondragon-Ramirez C, Vorobyov I, MacKerell A D and Pastor R W 2010 Update of the CHARMM all-atom additive force field for lipids: validation on six lipid types *J. Phys. Chem.* B **114** 7830–43
[21] Lim J B, Rogaski B and Klauda J B 2012 Update of the cholesterol force field parameters in CHARMM *J. Phys. Chem.* B **116** 203–10
[22] Jorgensen W L *et al* 1983 Comparison of simple potential functions for simulating liquid water *J. Chem. Phys.* **79** 926–35
[23] Marrink S J, Risselada H J, Yefimov S, Tieleman D P and de Vries A H 2007 The MARTINI force field: coarse grained model for biomolecular simulations *J. Phys. Chem.* B **111** 7812–24
[24] Zhang Q *et al* 2012 The stem region of premembrane protein plays an important role in the virus surface protein rearrangement during dengue maturation *J. Biol. Chem.* **287** 40525–34
[25] Hsin J, Gumbart J, Trabuco L G, Villa E, Qian P, Hunter C N and Schulten K 2009 Protein-induced membrane curvature investigated through molecular dynamics flexible fitting *Biophys. J.* **98** 321–9
[26] Humphrey W, Dalke A and Schulten K 1996 VMD: visual molecular dynamics *J. Mol. Graph. Model.* **14** 33–8
[27] Schrödinger L The PyMOL molecular graphics system, version 1.7.4
[28] Swift L L 1995 Assembly of very-low-density lipoproteins in rat-liver: a study of nascent particles recovered from the rough endoplasmic-reticulum *J. Lipid Res.* **36** 395–406
[29] Berendsen H J C, Postma J P M, Vangunsteren W F, Dinola A and Haak J R 1984 Molecular-dynamics with coupling to an external bath *J. Chem. Phys.* **81** 3684–90
[30] Hess B, Bekker H, Berendsen H J C and Fraaije J G E M 1995 LINCS: a linear constraint solver for molecular simulations *J. Comput. Chem.* **18** 1463–72
[31] Yesylevskyy S O, Schafer L V, Sengupta D and Marrink S J 2010 Polarizable water model for the coarse-grained MARTINI force field *PLoS Comput. Biol.* **6** e1000810
[32] Kandt C, Ash W L and Tieleman D P 2007 Setting up and running molecular dynamics simulations of membrane proteins *Methods* **41** 475–88
[33] Bussi G, Donadio D and Parrinello M 2007 Canonical sampling through velocity rescaling *J. Chem. Phys.* **126** 014101
[34] Bernstein F C, Koetzle T F, Williams G J B, Meyer E F, Brice M D, Rodgers J R, Kennard O, Shimanouchi T and Tasumi M 1977 Protein data bank—computer-based archival file for macromolecular structures *J. Mol. Biol.* **112** 535–42
[35] Jo S, Lim J B, Klauda J B and Im W 2009 CHARMM-GUI membrane builder for mixed bilayers and its application to yeast membranes *Biophys. J.* **97** 50–8
[36] Price D J and Brooks C L 2004 A modified TIP3P water potential for simulation with Ewald summation *J. Chem. Phys.* **121** 10096–103
[37] Lipowsky R 2013 Spontaneous tubulation of membranes and vesicles reveals membrane tension generated by spontaneous curvature *Faraday Discuss* **161** 305–31